Structure of excited states of ^{11}Be studied with antisymmetrized molecular dynamics

Y. Kanada-En'yo
Institute of Particle and Nuclear Studies, High Energy Accelerator Research Organization, 1-1 Oho, Tsukuba, Ibaraki 305-0801, Japan

H. Horiuchi
Department of Physics, Kyoto University, Kyoto 606-01, Japan

(Received 16 April 2002; published 2 August 2002)

The structures of the ground and excited states of ^{11}Be were studied with a microscopic method of antisymmetrized molecular dynamics. The theoretical results reproduce the abnormal parity of the ground state and predict various kinds of excited states. We suggest a new negative-parity band with a well-developed cluster structure which reaches high-spin states. Focusing on a 2α cluster structure, we investigated the structure of the ground and excited states. We point out that molecular orbits play important roles for the intruder ground state and the low-lying $2\hbar\omega$ states. The features of the breaking of α clusters were also studied with the help of data for Gamow-Teller transitions.

DOI: 10.1103/PhysRevC.66.024305 PACS number(s): 27.20.+n, 21.10.Pc, 23.40.−s

I. INTRODUCTION

Recently, information on the excited states of light unstable nuclei has increased rapidly [1–5]. In the excited states of light unstable nuclei, an exotic molecular structure of light unstable nuclei is one of the attractive subjects in experimental and theoretical research. For example, molecular structure has been suggested to appear in neutron-rich nuclei, such as ^{10}Be and ^{12}Be [1,4–12]. von Oertzen *et al.* [6,7] proposed a kind of exotic cluster structure with a $2\hbar\omega$ configuration in the excited states of ^{11}Be. However, there have been few microscopic studies on the excited states of ^{11}Be.

Needless to say, α-cluster cores are very important in the ground and excited states of ^{11}Be as well as in ^{9}Be and ^{10}Be. However, we should not forget the breaking of α clusters in ^{11}Be because there are many valence neutrons around the α clusters. The experimental data concerning the β-decay strength are very useful to estimate the breaking of the 2α-cluster structure in Be isotopes, because Gamow-Teller transitions from Li to Be are not allowed if the α-cluster cores in the daughter state of Be are completely ideal ones with a simple $(0s)^4$ configuration. It is very interesting that the recently measured β-decay strength from ^{11}Li to ^{11}Be indicates a significant breaking of α clusters in the excited states of ^{11}Be [2]. Therefore, it is important to also study the breaking of α clusters due to the surrounding neutrons as well as the development of clustering in ^{11}Be.

We should point out another interesting feature in ^{11}Be. Abnormal parity of the ground state in ^{11}Be has been known for a long time. Namely, the spin parity of the ground state is $1/2^+$, which seems to be inconsistent with the ordinary shell-model picture in which ^{11}Be with seven neutrons may have a $1/2^-$ state as the ground state. It has long been a problem why parity inversion occurs in ^{11}Be. As possible reasons for this parity inversion, such effects as the halo structure, a core deformation, clustering, and paring are suggested. For example, the energy gain of a positive-parity state of ^{11}Be is discussed in Refs. [13–17]. However, the ground-state structure has not been sufficiently studied by fully microscopic calculations without assumptions such as the existence of core nuclei. Although the cluster structure must be important in Be isotopes, it is difficult for mean-field approaches to describe developed cluster structures. With a theoretical method of antisymmetrized molecular dynamics, Doté *et al.* have studied the abnormal parity ground state of ^{11}Be without assuming cores or the stability of the mean field. However, in their work [8], the effects of angular momentum projections and three-body forces were approximately estimated by perturbative treatments.

Our aim is to make a systematic research of the structure of the ground and excited states of ^{11}Be based on microscopic calculations. An important point is that the theoretical approach should be free from such model assumptions as stability of the mean field and the existence of inert cores or clusters. First of all, traditional mean-field approaches are not useful to study the developed cluster structure in Be isotopes. With cluster models, the cluster structure of the excited states of ^{9}Be and ^{10}Be has been successfully explained [11,12,18–20] by assuming 2α cores and surrounding neutrons. Since the assumption of 2α-cluster cores is not appropriate to discuss the breaking of α cores, these cluster models are not sufficient for investigations of ^{11}Be with many valence neutrons. In fact, it is difficult to use them to directly calculate the experimental data of the β-decay strength from ^{11}Li. With these models it may not be possible to describe the recently discovered excited state at 8.04 MeV with the strong β transition strength from ^{11}Li.

We have applied a theoretical approach of antisymmetrized molecular dynamics (AMD). The AMD method has already proved to be useful for studying the structures of light nuclei [8,10,21–24]. Within this framework, we do not need such model assumptions as inert cores, clusters, or axial symmetries, because the basis wave functions of a nuclear system are written by Slater determinants where all centers of the Gaussian-type spatial part of single-particle wave functions are free parameters. In AMD studies of neutron-rich nuclei, we investigated the structures of Be isotopes [8,22,24]. In AMD calculations, many kinds of experimental

data for nuclear structure have been reproduced. As a result of the flexibility of the AMD wave function, we have succeeded in describing the structure changes between shell-model-like states and cluster states with an increase in the neutron number. In previous studies [8,22] of Be isotopes, the excited states of ^{11}Be were not studied in detail because the calculations are based on the variation before a total angular momentum projection. Recently, the AMD framework has been developed to be an extended version based on variational calculations after a spin-parity projection (variation after projection: VAP), which has already been confirmed to be powerful for studying the excited states of light nuclei. The method has been applied to a stable nucleus ^{12}C [23] and to unstable nuclei ^{10}Be, ^{12}Be, and ^{14}Be [9,10,25].

In the present work, the structures of the ground and excited states of ^{11}Be were studied by performing VAP calculations using the AMD method. In the next section (Sec. II), we explain the formulation of AMD for a nuclear structure study of the ground and excited states. The adopted effective interactions are briefly explained in Sec. III. In Sec. IV, we present the theoretical results concerning the energy levels, β decays and $E2$ transitions compared with the experimental data. We predict a new rotational band with a well-developed cluster structure which comes from $2\hbar\omega$ configurations. In Sec. V, the intrinsic structure and behavior of the valence neutrons are discussed. We also discuss the breaking of α clusters, which has an important effect on the β-decay strength. Finally, we summarize our work in Sec. VI.

II. FORMULATION

In this section, the formulation of AMD for a nuclear structure study of the excited states is briefly explained. For more detailed descriptions of the AMD framework the reader is referred to Refs. [10,22,23].

A. Wave function

An AMD wave function of a nucleus with mass number A is a Slater determinant of Gaussian wave packets:

$$\Phi_{AMD}(\mathbf{Z}) = \frac{1}{\sqrt{A!}}\mathcal{A}\{\varphi_1, \varphi_2, \ldots, \varphi_A\}, \tag{1}$$

$$\varphi_i = \phi_{\mathbf{X}_i}\chi_{\xi_i}\tau_i : \begin{cases} \phi_{\mathbf{X}_i}(\mathbf{r}_j) \propto \exp\left[-\nu\left(\mathbf{r}_j - \frac{\mathbf{X}_i}{\sqrt{\nu}}\right)^2\right], \\ \chi_{\xi_i} = \begin{pmatrix} \frac{1}{2}+\xi_i \\ \frac{1}{2}-\xi_i \end{pmatrix}, \end{cases} \tag{2}$$

where the ith single-particle wave function φ_i is a product of the spatial wave function $\phi_{\mathbf{X}_i}$, the intrinsic spin function χ_{ξ_i} and the isospin function τ_i. The spatial part $\phi_{\mathbf{X}_i}$ is presented by a Gaussian wave packet whose center is defined by complex parameters X_{1i}, X_{2i}, X_{3i}. Here χ_{ξ_i} is the intrinsic spin function parametrized by ξ_i, while τ_i is the isospin function, which is fixed to be up (proton) or down (neutron) in the present calculations. Thus an AMD wave function is parametrized by a set of complex parameters $\mathbf{Z} \equiv \{X_{ni}, \xi_i\}$ ($n=1,3$ and $i=1,A$). $\mathbf{X}_i$ are the centers of Gaussians for the spatial parts and the parameters ξ_i's determine the directions of the intrinsic spins of the single particle wave functions.

If we consider a parity eigenstate projected from an AMD wave function, the total wave function consists of two Slater determinants,

$$\Phi(\mathbf{Z}) = (1 \pm P)\Phi_{AMD}(\mathbf{Z}), \tag{3}$$

where P is a parity projection operator. In the case of a total angular momentum projection (J projection), the wave function of a system is represented by the integral of the rotated states,

$$\Phi(\mathbf{Z}) = P^J_{MK'}\Phi_{AMD}(\mathbf{Z}) = \int d\Omega D^{J*}_{MK'}(\Omega) R(\Omega)\Phi_{AMD}(\mathbf{Z}), \tag{4}$$

where the function D^J_{MK} is the well-known Wigner's D function and $R(\Omega)$ stands for the rotation operator with Euler angle Ω.

In principal the total wave function can be a superposition of independent AMD wave functions. For example, a system is written by a superposition of spin-parity-projected AMD wave functions $P^{J\pm}_{MK'}\Phi_{AMD}$ as follows:

$$\Phi = cP^{J\pm}_{MK'}\Phi_{AMD}(\mathbf{Z}) + c' P^{J\pm}_{MK'}\Phi_{AMD}(\mathbf{Z}') + \cdots. \tag{5}$$

The expectation values of a given tensor operator T^k_q (rank k) for the total-angular-momentum-projected states $P^{J_1\pm}_{M_1K_1}\Phi_{AMD}(\mathbf{Z})$ and $P^{J_2\pm}_{M_2K_2}\Phi_{AMD}(\mathbf{Z}')$ are calculated as follows:

$$\langle P^{J_1}_{M_1K_1}\Phi_1 | T^k_q | P^{J_2}_{M_2K_2}\Phi_2\rangle \tag{6}$$

$$= \frac{2J_2+1}{8\pi^2}(J_2M_2kq|J_1M_1)\sum_{K\nu}(J_2Kk\nu|J_1K_1) \times \int d\Omega D^{J_2*}_{KK_2}(\Omega)\langle\Phi_1|T^k_\nu R(\Omega)|\Phi_2\rangle. \tag{7}$$

The three-dimensional integral can be evaluated numerically by taking a finite number of mesh points of the Euler angle $\Omega = (\alpha, \beta, \gamma)$.

B. Energy variation

We make variational calculations for a trial wave function to find the state which minimizes the energy of the system,

$$\frac{\langle\Phi|H|\Phi\rangle}{\langle\Phi|\Phi\rangle}. \tag{8}$$

In the AMD framework, the energy variation is performed by a method of frictional cooling, one of the imaginary time methods. Regarding the frictional cooling method, the reader

is referred to Refs. [21,22]. The time development of the parameters $\mathbf{Z}$ of a wave function $\Phi(\mathbf{Z})$ is simulated by the frictional cooling equations

$$\frac{dX_{nk}}{dt}=(\lambda+i\mu)\frac{1}{i\hbar}\frac{\partial}{\partial X^{*}_{nk}}\frac{\langle\Phi(\mathbf{Z})|H|\Phi(\mathbf{Z})\rangle}{\langle\Phi(\mathbf{Z})|\Phi(\mathbf{Z})\rangle}$$

$$(n=1,3,\quad k=1,A), \tag{9}$$

$$\frac{d\xi_{k}}{dt}=(\lambda+i\mu)\frac{1}{i\hbar}\frac{\partial}{\partial \xi^{*}_{k}}\frac{\langle\Phi(\mathbf{Z})|H|\Phi(\mathbf{Z})\rangle}{\langle\Phi(\mathbf{Z})|\Phi(\mathbf{Z})\rangle}$$

$$(k=1,A), \tag{10}$$

with arbitrary real numbers λ and $\mu<0$. It is easily proved that the energy of the system decreases with each time step due to the frictional term μ. After sufficient cooling iterations, the parameters for the minimum-energy state are obtained.

C. Wave function for $J^{\pm}$ states

In order to obtain the wave function for a $J^{\pm}$ state, we make the energy variation after a spin-parity projection (VAP) for an AMD wave function by using the frictional cooling method explained above. That is to say we perform the energy variation for the trial function $\Phi=P^{J^{\pm}}_{MK'}\Phi_{AMD}(\mathbf{Z})$, the spin-parity eigenstate projected from an AMD wave function. First we make variational calculations after only the parity projection, but before the spin projection (variation before projection: VBP), to prepare an initial trial wave function $\Phi_{AMD}(\mathbf{Z}_{init})$. After obtaining an initial wave function by VBP calculations, we evaluate the expectation values of the Hamiltonian for the spin-parity-projected states by choosing the body-fixed 3-axis for the Ω rotation to be the approximate principal z axis on the intrinsic deformation. Then, we find an appropriate K' quantum that gives the minimum diagonal energy of the spin-parity eigenstate,

$$\frac{\langle P^{J^{\pm}}_{MK'}\Phi_{AMD}(\mathbf{Z}_{init})|H|P^{J^{\pm}}_{MK'}\Phi_{AMD}(\mathbf{Z}_{init})\rangle}{\langle P^{J^{\pm}}_{MK'}(\mathbf{Z}_{init})|P^{J^{\pm}}_{MK'}(\mathbf{Z}_{init})\rangle}, \tag{11}$$

where $K'=\langle J_3\rangle$. For each spin parity $J^{\pm}$, we start VAP calculations for the normalized energy expectation value $\langle P^{J^{\pm}}_{MK'}\Phi_{AMD}(\mathbf{Z})|H|P^{J^{\pm}}_{MK'}\Phi_{AMD}(\mathbf{Z})\rangle/\langle P^{J^{\pm}}_{MK'}(\mathbf{Z})|P^{J^{\pm}}_{MK'}(\mathbf{Z})\rangle$, with the adopted K' quantum from the initial state. In general, the direction of the approximately principal z axis is automatically determined in the energy variation because the shape of the intrinsic system can vary freely. The approximately principal axis can deviate from the 3-axis in the VAP procedure with a given $K'=\langle J_3\rangle$. That is to say, the optimum state $P^{J^{\pm}}_{MK'}\Phi_{AMD}$, obtained after the variation, may contain so-called K-mixing ($K=\langle J_z\rangle$) components. However, the deviation of the z axis from the 3-axis is found to be small in many cases. This means that the obtained states do not contain K-mixing components so much, and K' well corresponds to the K quantum.

Concerning the states in the lowest band with each parity, we can obtain appropriate initial wave functions by simple VBP calculations, as mentioned above. For the highly excited states, in order to obtain initial wave functions and appropriate K' quanta for VAP calculations, we make VBP calculations with a constraint on the AMD wave function. The details of the AMD calculation with constraints are described in Ref. [21]. In the present calculations, we adopted a constraint as the expectation value of the total-oscillator quanta to equal a given number. After choosing a corresponding K' quantum, we performed VAP calculations from the initial wave function. When we obtained other local minimum states than the obtained states, we considered them as states in higher rotational bands.

D. Diagonalization

After the VAP calculations for the $J^{\pm}_{n}$ states, the optimum intrinsic states $\Phi^{1}_{AMD},\Phi^{2}_{AMD},\ldots,\Phi^{m}_{AMD}$ are obtained. Here, m indicates the number of calculated levels. We consider that the obtained wave functions approximately represent the intrinsic wave functions of the $J^{\pm}_{n}$ states. We determine the final wave functions by superposing the obtained AMD wave functions. That is to say, we determine the coefficients $c,c',\ldots$ in Eq. (5) for each $J^{\pm}_{n}$ state by diagonalizing the Hamiltonian matrix $\langle P^{J^{\pm}}_{MK'}\Phi^{i}_{AMD}|H|P^{J^{\pm}}_{MK''}\Phi^{j}_{AMD}\rangle$ and the norm matrix $\langle P^{J^{\pm}}_{MK'}\Phi^{i}_{AMD}|P^{J^{\pm}}_{MK''}\Phi^{j}_{AMD}\rangle$ simultaneously with regard to (K',K'') and (i,j). In comparison with the experimental data, such as the energy levels and the strength $E2$ transitions, the theoretical values are calculated with the final states after diagonalization.

III. INTERACTIONS

The adopted interaction for the central force is case 3 of the MV1 force [26], which contains a zero-range three-body term, $V^{(3)}$, in addition to the two-body interaction $V^{(2)}$,

$$V_{DD}=V^{(2)}+V^{(3)}, \tag{12}$$

$$V^{(2)}=\sum_{i<j}(1-m+bP_{\sigma}-hP_{\tau}-mP_{\sigma}P_{\tau})\times\left\{V_{A}\exp\left[-\left(\frac{|\mathbf{r}_i-\mathbf{r}_j|}{r_A}\right)^2\right]+V_{R}\exp\left[-\left(\frac{|\mathbf{r}_i-\mathbf{r}_j|}{r_R}\right)^2\right]\right\}, \tag{13}$$

$$V^{(3)}=\sum_{i<j<k}v^{(3)}\delta(\mathbf{r}_i-\mathbf{r}_j)\,\delta(\mathbf{r}_i-\mathbf{r}_k), \tag{14}$$

where P_{σ} and P_{τ} stand for the spin and isospin exchange operators, respectively. As for the two-body spin-orbit force V_{LS}, we use the G3RS force [27] as follows:

$$V_{LS}=\sum_{i<j}\{u_I\exp(-\kappa_I r^2)+u_{II}\exp(-\kappa_{II}r^2)\}\times\frac{(1+P_\sigma)}{2}\frac{(1+P_\tau)}{2}\mathbf{l}\cdot(\mathbf{s}_i+\mathbf{s}_j). \quad (15)$$

The Coulomb interaction V_C is approximated by a sum of seven Gaussians. The total interaction V is the sum of these interactions: $V=V_{DD}+V_{LS}+V_C$.

IV. RESULTS

The structures of the excited states of ^{11}Be were studied based on VAP calculations in the framework of AMD. In this section we present the theoretical results concerning the energy levels, the $E2$ transitions, and the β transitions, which should be directly compared with the experimental data. More detailed discussions of the intrinsic structures are given in the next section.

We adopted two sets of the interaction parameters. One parameter set (1) was $m=0.65$, $b=h=0$ for the Majorana, Bartlett, and Heisenberg terms in the central force and $u_I=-u_{II}=3700$ MeV for the strength of the spin-orbit forces, which were used in a previous study on the excited states of ^{10}Be. We also tried another set (2) with weaker spin-orbit forces as $u_I=-u_{II}=2500$ MeV. Other parameters in case (2) were the same as those in case (1). The width parameter ν was chosen to be 0.18 fm^{-2}, which gave the minimum energy of ^{11}Be in a VBP calculation.

In VBP calculations we know that the lowest positive-parity band $K^\pi=1/2^+$ consists of $1/2^+$, $3/2^+$, $5/2^+$, $7/2^+$, and $9/2^+$ states and the lowest negative-parity band $K^\pi=1/2^-$ consists of $1/2^-$, $3/2^-$, and $5/2^-$ states. Therefore, the $J_1^\pm$ states in the lowest bands were obtained by VAP calculations for $P^{J^\pm}_{MK'}\Phi_{AMD}$ with the corresponding $(J^\pm,K')$ values as $(1/2^+,1/2)$, $(3/2^+,1/2)$, $(5/2^+,1/2)$, $(7/2^+,1/2)$, $(9/2^+,1/2)$, $(1/2^-,1/2)$, $(3/2^-,1/2)$, and $(5/2^-,1/2)$. We calculated the higher excited states in the second negative-parity band by VAP calculations with $(J^\pm,K')=(7/2^-,3/2)$, $(9/2^-,3/2)$, $(11/2^-,3/2)$, $(13/2^-,3/2)$, ... These states are considered to belong to a band with $K^\pi=3/2^-$. After obtaining the intrinsic states in this second negative-parity band for $J\geqslant 7/2$, the excited $J^\pm=3/2^-_2$ and $5/2^-_2$ states in $K^\pi=3/2^-$ were found as local minima with VAP calculations by starting from the intrinsic states obtained for the higher-spin states. In order to find the other excited $3/2^-$ state, we performed VAP calculations for the spin-parity-projected AMD wave function with fixed intrinsic spin directions as three spin-down protons, one spin-up proton, four spin-down, and four spin-up neutrons. The obtained wave function for the $3/2^-$ state is dominated by a component of the total intrinsic spin $S_p=1$ for protons. We superposed the wave functions to calculate the final wave functions by diagonalizing the Hamiltonian matrix.

We should notice that all possible excited states were not exhausted in the present calculations. In this work we performed VAP calculations basically for the rotational states which can be known from VBP calculations with or without constraint. For the higher excited states we must extend the VAP calculations with the orthogonal condition to the lower states by superpositions, as in previous studies [10,23]. Above the states shown in the present results, there should exist other excited states which may be obtained by extended VAP calculations.

A. Energies

The theoretical binding energies of ^{11}Be are 58.2 MeV in case (1) and 54.4 MeV in case (2), both of which underestimate the experimental value 65.48 MeV. The binding energy can be reproduced by choosing an interaction parameter, such as $m=0.60$, of the Majorana term. However, unfortunately, it is difficult to reproduce all of the features of nuclear structures, such as the binding energies, energy levels, radii, deformations, and so on with one set of interaction parameters. Since we studied the excited states by taking care of the excitation energies and the intrinsic structures, we adopted the case (1) interaction, which well reproduces the features of the excited states of ^{10}Be [10], except for the binding energy. With this interaction, the spin-parity $1/2^+$ of the ground state of ^{11}Be can be described by the present calculations. We also used another interaction case (2) with weaker spin-orbit forces to be compared. Improving the effective interactions is one of the important problems of nuclear studies to be solved.

Here, we comment on the stability of AMD wave functions above the threshold energies. Since the single-particle wave functions are written by Gaussians in AMD calculations, the relative motion between particles in a system is restricted by a Gaussian or a linear combination of Gaussians. Because of the limitation of the model space, neither continuum states nor outgoing waves can be represented in the present model. Even if the energy of a nucleus is above the threshold energies of particle decays, the particles cannot necessarily go away in the present framework. In this sense, the system is treated in the bound-state approximation. The widths for the particle decays should be carefully discussed based on other frameworks, such as a method with a reduced width amplitude or a complex scaling method beyond the present AMD framework.

The energy levels of ^{11}Be are shown in Fig. 1. There are many low-lying levels in the experimental data. The abnormal spin-parity $1/2^+$ of the ground state has been known, although the normal spin parity of ^{11}Be is $1/2^-$ in the simple shell-model picture. The calculations with the case (1) interaction reproduce the parity inversion between $1/2^+$ and $1/2^-$ states. In the theoretical results, the rotational bands $K^\pi=1/2^+$ and $K^\pi=1/2^-$ start from the band head $1/2^+$ and $1/2^-$ states, respectively. Also, in the results with the case (2) interaction, the $1/2^+$ state is lowest in the $K^\pi=1/2^+$ band; however, it is slightly higher than the negative-parity $1/2^-$ state by 1.4 MeV. As a result, the abnormal parity of the ground state cannot be reproduced by the case (2) interaction, in which the spin-orbit forces are weaker than those in case (1). We should not conclude that the calculations with the case (1) interaction are better than those in case (2), because the neutron halo effect on the energy gain of the

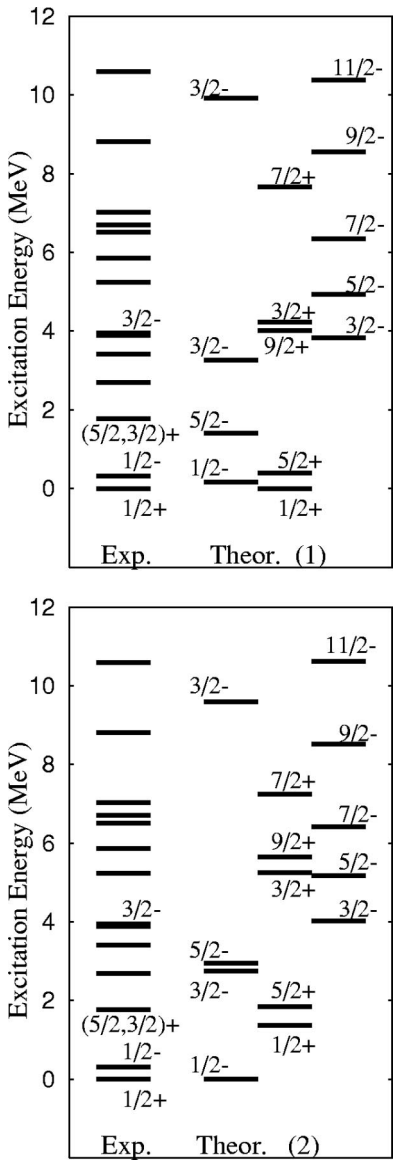

FIG. 1. Excitation energies of the excited states of ^{11}Be. Theoretical results for case (1) and case (2) interactions are compared with the experimental data quoted from the *Table of Isotopes*.

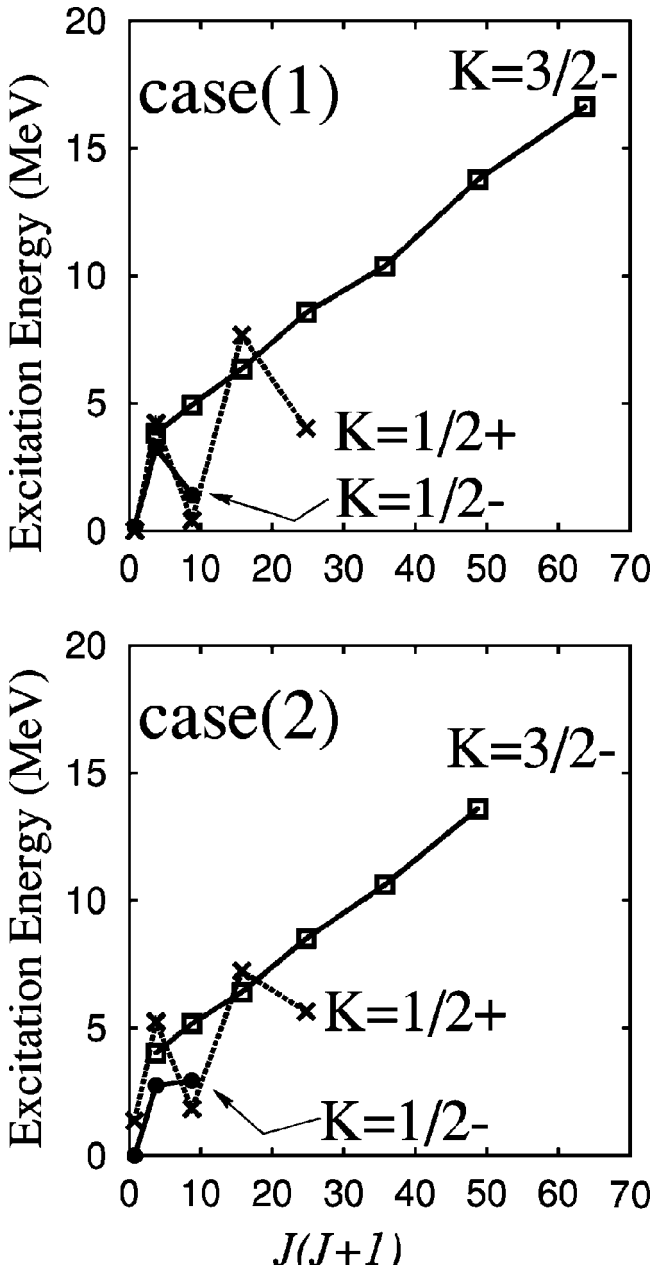

FIG. 2. Excitation energies of the rotational bands of ^{11}Be as a function of $J(J+1)$. The lines indicate the theoretically obtained rotational bands $K^\pi=1/2^-$, $K^\pi=1/2^+$, $K^\pi=3/2^-$.

$1/2^+$ state is not taken into account in the present calculations. The details of the reproduction of parity inversion with the case (1) interaction are described in a later section.

In results for both case (1) and case (2), there exist some rotational bands in the low-energy region. By classifying the calculated excited states we could obtain three rotational bands $K^\pi=1/2^+$, $K^\pi=1/2^-$, and $K^\pi=3/2^-$, which are dominated by $1\hbar\omega$, $0\hbar\omega$, and $2\hbar\omega$ neutron configurations, respectively. In Fig. 2, we show the excitation energies of the rotational bands as a function of the total spin $J(J+1)$. We find a new eccentric band, $K^\pi=3/2^-$, which starts from the second $3/2^-$ state at about 4 MeV. The excited states in the $K^\pi=3/2^-$ band are dominated by $2\hbar\omega$ excited configurations with two particles and three holes ($2p$-$3h$) in neutron shells. The $K^\pi=3/2^-$ band is constructed by a well-deformed intrinsic state with a developed cluster structure. The rotational band indicates a large moment of inertia and reaches the high-spin states at about 20 MeV. The highest spin is $15/2^-$ in case (1) and $13/2^-$ in case (2). In VAP calculations with further high spins, we cannot obtain any stable states, since an α particle escapes far away in the variational calculations. This means that the energy of the relative motion between clusters is beyond the classical barrier due to the Coulomb and centrifugal forces. Since the barrier height is very sensitive to the binding energy, we examined the highest spin of the $K^\pi=3/2^-$ band with another set of interaction parameters while taking care of the binding energy of ^{11}Be. If we change the Majorana exchange term of case (1) to $m=0.60$, we can make the system bound as deeply as the experimental binding energy. Then, a $17/2^-$

state is obtained as the highest-spin state. von Oertzen *et al.* suggested some candidates for the states belonging to this new negative-parity band in the experimental data observed in the two-neutron transfer reactions ^{9}Be(^{13}C, ^{11}C)^{11}Be [7]. Although they suggested a possibility of a $19/2^-$ state, the present results are negative to such a high-spin state as $19/2^-$ in the rotational $K^\pi=3/2^-$ band, because $17/2^-$ is the highest spin made from the $2p$-$3h$ configurations. It should be noted that the present work is the first microscopic calculation which predicts the $K^\pi=3/2^-$ band with a well-developed cluster structure. Since ^{11}Be is a loosely bound system, further studies taking account of the widths of the excited states are necessary to determine the band terminal.

We find an excited $3/2^-$ state at about 10 MeV (Fig 1). In this state, the proton structure is quite strange compared with the other excited states of ^{11}Be. In most of the states of ^{11}Be, we find 2α cores as well as other Be isotopes: ^{8}Be, ^{9}Be, and ^{10}Be. However, in the $3/2^-$ state at 10 MeV, only one α cluster is formed. The other two protons do not form an α cluster, but couple to be totally $S=1$ with aligned intrinsic spins. It is an analogue with the structure of the first 1^+ state with the unnatural spin parity in ^{12}C. We consider that this $3/2^-$ state must be a newly measured state at 8.04 MeV [2] to which the β-decay transition from ^{11}Li is strong. Although its excitation energy was overestimated in the present calculations, it can be easily improved by changing parameters b and h of the Bartlett and Heisenberg terms. For example parameters $b=-0.2$, $h=0.4$, $m=0.41$ give a 2 MeV lower excitation energy of the $3/2^-$ state than that with $b=0.0$, $h=0.0$, $m=0.65$. Here, we fit the Majorana parameter m so as to give the same α-α interaction as in case (1). The change of parameters has no significant effect on the excitation energies of the other states with 2α clusters. The results indicate that the Bartlett and Heisenberg terms should be taken into consideration in the detailed study of the energy levels, though they have often been omitted in the traditional work on stable nuclei.

B. Transition strength

Data concerning the β-decay strength are very useful to investigate the structures of excited states. There are many experimental data concerning the β^- and β^+ decays into the excited states of ^{11}Be. The strength of the β^- decays from ^{11}Li has recently been measured [2]. For β^+ decays, the strength of the Gamow-Teller (GT) transitions has been deduced from the charge-exchange reactions ^{11}B(t,^{3}He)^{11}Be [3]. In the GT transitions from ^{11}Li($3/2^-$) and ^{11}B($3/2^-$), the allowed daughter states are the $1/2^-$, $3/2^-$, or $5/2^-$ states. In Table I the experimental log(ft) values are presented comparing with the theoretical results. In order to calculate the log(ft) values of GT transitions into the excited states of ^{11}Be we prepared the parent states ^{11}Li($3/2^-$) and ^{11}B($3/2^-$) by VAP calculations within the same framework.

The experimental log(ft) values were reproduced well by theoretical calculations. It is easily understood that the decays into the excited states in the $K^\pi=3/2^-$ band are weak because these states have well-developed cluster structures with dominant $2\hbar\omega$ components, which make the overlap of a GT operator with the parent state of ^{11}B small. On the other hand, we consider that three levels at 0.32 MeV, 2.69 MeV, and 3.96 MeV measured in the β^+ transitions correspond to the states $1/2^-_1$, $3/2^-_1$, and $5/2^-_1$ in the $K^\pi=1/2^-$ band because the experimental data indicate significant β^+ strength as log(ft) <5.0, which is consistent with the theoretical results.

TABLE I. Log(ft) values of the β transitions. The theoretical values are obtained from the Gamow-Teller transition strength. The experimental data of β decays from ^{11}Li are taken from Ref. [2]. The log ft values concerning the Gamow-Teller transition from ^{11}B are deduced from the charge-exchange reactions [3].

Transitions	log ft Theory (1)	Theory (2)
^{11}Li($3/2^-$)$\rightarrow$^{11}Be($1/2^-_1$)	5.0	5.5
^{11}Li($3/2^-$)$\rightarrow$^{11}Be($3/2^-_1$)	4.4	5.0
^{11}Li($3/2^-$)$\rightarrow$^{11}Be($5/2^-_1$)	4.5	5.0
^{11}Li($3/2^-$)$\rightarrow$^{11}Be($3/2^-_2$)	4.9	6.2
^{11}Li($3/2^-$)$\rightarrow$^{11}Be($3/2^-_3$)	3.9	4.3
^{11}B($3/2^-$)$\rightarrow$^{11}Be($1/2^-_1$)	3.9	4.2
^{11}B($3/2^-$)$\rightarrow$^{11}Be($3/2^-_1$)	3.8	4.3
^{11}B($3/2^-$)$\rightarrow$^{11}Be($5/2^-_1$)	4.2	5.0
^{11}B($3/2^-$)$\rightarrow$^{11}Be($3/2^-_2$)	4.5	5.5
^{11}B($3/2^-$)$\rightarrow$^{11}Be($3/2^-_3$)	4.3	5.4
Transitions	Expt.	
^{11}Li($3/2^-$)$\rightarrow$^{11}Be($1/2^-_1$, 0.32 MeV)	5.67(4)	
^{11}Li($3/2^-$)$\rightarrow$^{11}Be(2.69 MeV)	4.87(8)	
^{11}Li($3/2^-$)$\rightarrow$^{11}Be(3.96 MeV)	4.81(8)	
^{11}Li($3/2^-$)$\rightarrow$^{11}Be(5.24 MeV)	5.05(8)	
^{11}Li($3/2^-$)$\rightarrow$^{11}Be(8.04 MeV)	4.43(8)	
Transitions	Expt.	
^{11}B($3/2^-$)$\rightarrow$^{11}Be($1/2^-_1$, 0.32 MeV)	4.3(1)	
^{11}B($3/2^-$)$\rightarrow$^{11}Be(2.69 MeV)	4.4(1)	
^{11}B($3/2^-$)$\rightarrow$^{11}Be(3.96 MeV)	4.8(2)	

What is important concerning the β^- decays from ^{11}Li is that the strength is very sensitive to the breaking of 2α-cluster cores in ^{11}Be. If the daughter state of ^{11}Be possesses two ideal α-cluster cores with $(0s)^4$ configurations, the GT transitions from ^{11}Li are completely forbidden because of the Pauli principle. In other words, the strength of the GT transitions from ^{11}Li indicates the degree of α-cluster breaking in the daughter states of ^{11}Be. From this point of view, one of the reasons for the weak β^- transitions as log(ft)=5.67 to the lowest $1/2^-$ state at 0.32 MeV is the 2α-cluster structure in ^{11}Be($1/2^-$). Another reason for the weak β^- transitions has been suggested to be the effect of the halo structure in ^{11}Li by Suzuki and Otsuka [28]. The ground state of ^{11}Li is known to have a neutron halo structure which originates from s orbits. The mixing of the s orbits causes weak β^- transitions to the normal states of ^{11}Be. Since the halo structure of ^{11}Li cannot be described with the present AMD wave function, the possible halo effects on the β^- decays are not included in the present results. If we suppose the mixing ratio of the s orbits in the ground ^{11}Li state to be 50%, the theoretical log(ft) values concern-

TABLE II. $E2$ strength of ^{11}Be. The theoretical results of AMD with the interactions of case (1) are listed.

Transitions	Present results (e^2 fm^4)
^{11}Be;$3/2_1^- \rightarrow 1/2_1^-$	9
^{11}Be;$5/2_1^- \rightarrow 1/2_1^-$	8
^{11}Be;$5/2_1^- \rightarrow 3/2_1^-$	2
^{11}Be;$5/2_2^- \rightarrow 3/2_2^-$	37
^{11}Be;$7/2_1^- \rightarrow 3/2_2^-$	14
^{11}Be;$7/2_1^- \rightarrow 5/2_2^-$	25
^{11}Be;$5/2_1^+ \rightarrow 1/2_1^+$	14
^{11}Be;$5/2_1^+ \rightarrow 3/2_1^+$	7
^{11}Be;$3/2_1^+ \rightarrow 1/2_1^+$	13
^{11}Be;$5/2_2^- \rightarrow 3/2_1^-$	7
^{11}Be;$3/2_2^- \rightarrow 3/2_1^-$	8
^{11}Be;$3/2_2^- \rightarrow 1/2_1^-$	2

ing the β^- decays into $1/2_1^-$, $3/2_1^-$, and $5/2_1^-$ are expected to be increased by log(2)$\sim$0.3 due to mixing. Even if we add 0.3 of the halo effect by hand to the present log(ft) values for $3/2_1^-$ and $5/2_1^-$ states, the log(ft) values in case (1) are still smaller than 5.0, because of sufficient cluster breaking. They are consistent with the experimentally measured rather small log ft values for decays to ^{11}Be (2.7 MeV) and ^{11}Be (3.9 MeV). In other words, the experimental data indicate a significant breaking of 2α-cluster cores in these states (2.7 and 3.9 MeV), which we consider to be the excited states $3/2_1^-$ and $5/2_1^-$.

In recent measurements of β^- decays, a new excited state at 8.04 MeV with strong β^- transitions has been discovered. The calculated log(ft) values for the $3/2^-$ state of ^{11}Be at about 10 MeV well corresponds to this newly observed state at 8.04 MeV. The transition is strong because the 2α-cluster structure completely disappears in this state.

As shown in Table I, the experimental data concerning the strength of β^- decays have been systematically reproduced in the present calculations. Considering the increases of log ft due to the halo effect of ^{11}Li, the theoretical values of log ft for β^- calculated with the case (1) interaction well agree with the experimental data. The reason for the good reproduction is because the significant breaking of 2α clusters in ^{11}Be is described in the present calculations. This is the same reason as in previous studies of ^{12}C, in which the experimental data concerning the strength of β^- and β^+ decays have been well reproduced. A quantitative discussion of the 2α-core breaking is given in the next section.

In Table II, we show the theoretical $B(E2)$ values. It has been proved that AMD calculations well reproduce the $B(E2)$ values of light neutron-rich nuclei. As shown in previous studies [9,22,23], the experimental Q moments and $B(E2)$ values of various nuclei have been well reproduced by using the bare charges in the AMD framework because of the advantage of the AMD method, which can directly describe proton deformations. Also, in the present results, the features of proton-matter deformations in the intrinsic states are reflected in the theoretical $B(E2)$ values. In the lowest negative-parity band $K^\pi = 1/2^-$, the intrinsic system deforms

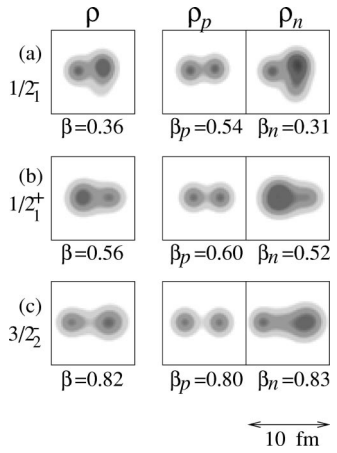

FIG. 3. Density distributions of the intrinsic structures of the $1/2_1^-$, $1/2_1^+$, $3/2_2^-$ states calculated with the case (1) interaction. The intrinsic system is projected on to a plane which contains the longitudinal axis of the intrinsic states. The density is integrated along a transverse axis perpendicular to the plane. The density distributions for matter, protons, and neutrons are presented in the left, middle, and right, respectively.

because of 2α-cluster cores, although the development of clustering is smallest compared with the other bands. The $B(E2)$ values are larger in the ground $K^\pi = 1/2^+$ band, which has a developed cluster structure with a large deformation. The $B(E2)$ values are enhanced between the states in the second negative-parity band, $K^\pi = 3/2^-$, with an extremely large deformation due to cluster development.

The $E1$ transition strength from $1/2_1^-$ to $1/2_1^+$ in ^{11}Be is known to be very large compared with those in other light nuclei. The theoretical value of $B(E1; 1/2_1^- \rightarrow 1/2_1^+) = 0.02$ e fm is much smaller than the experimentally observed strength 0.116 ± 0.011 e fm. The halo structure may have an important effect on the $E1$ strength.

V. DISCUSSIONS

We investigated the structures of ^{11}Be while focusing on the clustering aspects. It is found that two α-cluster cores are formed in most of the states of ^{11}Be as well as in other Be isotopes: ^{8}Be, ^{9}Be, ^{10}Be. In this section, we discuss the development of clustering and consider the roles of valence neutrons in the clustering states. We analyze the breaking of cluster cores and also describe the feature of a nonclustering state. The problem of parity inversion between positive- and negative-parity states is also discussed.

A. Cluster structure

We consider the intrinsic structures of the excited states while focusing on the clustering aspects. Although the states $P^{J^\pm}_{MK}\Phi^i_{AMD}$ are superposed for all of the obtained wave functions Φ^i_{AMD} so as to diagonalize the Hamiltonian matrix, the $J^\pm$ state after diagonalization is found to be dominated by the AMD wave function $P^{J^\pm}_{MK}\Phi^j_{AMD}$, which was obtained in a VAP calculation for the given spin and parity $J^\pm$. There-

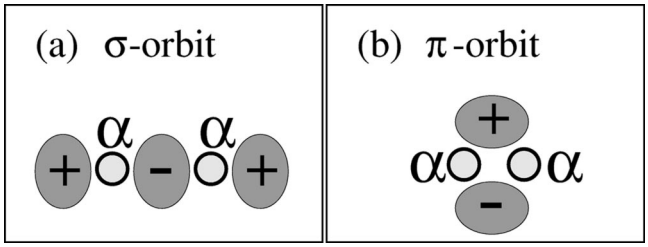

FIG. 4. Sketches for the molecular orbits, (a) σ orbits and (b) π orbits surrounding 2α's. The molecular orbits are understood by linear combinations of *p*-shell orbits around the α clusters.

fore, we consider the obtained AMD wave function Φ_{AMD}, with a VAP calculation as the intrinsic wave function of the corresponding $J^{\pm}$ state.

In the excited states, three rotational bands ($K^{\pi}=1/2^{+}$, $1/2^{-}$, $3/2^{-}$) are recognized, because the intrinsic structures of the states in each band are similar. The density distributions of the intrinsic states of the bandhead states ($1/2_1^{-}$, $1/2_1^{+}$, $3/2_2^{-}$) are shown in Fig. 3. The neutron structure of an intrinsic state is very different from those of the other rotational bands. As for the neutron deformation, the $1/2^{-}$ state has an oblate deformation. The oblate shape is natural in the normal-parity state in a system with neutron number $N=7$. In the $1/2^{+}$ state, the neutron density deforms prolately. The prolate deformation of the neutron density is extremely enhanced in the $3/2_2^{-}$ state. The single-particle behavior of neutrons is discussed in the next subsection.

In the proton density shown in Fig. 3, we can see dumbbell shapes due to two pairs of protons. Roughly speaking, this indicates that 2α cores are formed in all of the intrinsic states of these three rotational bands. The spatial development of clusters is small in the lowest negative-parity $1/2^{-}$ state, which has a main component of a normal $0\hbar\omega$ configuration. In the ground $1/2^{+}$ state with the abnormal parity, the 2α cluster structure develops. It is interesting that the most remarkable cluster structure is seen in the $3/2_2^{-}$ state, which belongs to the $K^{\pi}=3/2^{-}$ band. In this state, the 2α-cluster structure develops following the prolate deformation of the neutron density to have the largest intercluster distance among these three rotational bands. As a result of the development of 2α clustering, the proton deformation is larger in the $K^{\pi}=1/2^{+}$ band than in the $K^{\pi}=1/2^{-}$ band and largest in the $K^{\pi}=3/2^{-}$ band. The proton deformations are reflected in the theoretical $B(E2)$ values, as mentioned in the previous section. It should be pointed out that, in the $K^{\pi}=3/2^{-}$ band, the developed deformation decreases and the clustering weakens at the band terminal state with an increase of the spin near the highest spin, $J=15/2^{-}$.

B. Behavior of valence neutrons

As mentioned above, the deformation of the neutron density changes drastically between the rotational bands. In order to study the behavior of valence neutrons, we inspect the single-particle wave functions of the intrinsic states while focusing on the molecular orbits.

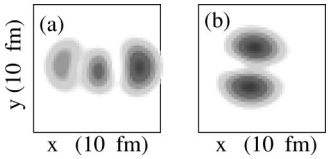

FIG. 5. Density distribution of single-neutron wave functions in the intrinsic system of the $1/2_1^{+}$ state calculated with case (1). (a) shows the density for the highest neutron orbit with the 90% positive-parity component, while (b) is for the second neutron orbit which contains 90% of a negative-parity component.

In Be isotopes, it has been known that the molecular orbits around 2α play important roles. The molecular orbits in Be isotopes have been suggested in ^{9}Be with $2\alpha+n$ cluster models [19]. von Oertzen *et al.* proposed a picture of Be dimers [6,7] to understand the excited states of neutron-rich Be isotopes. They predicted σ and π orbits which are made from linear combinations of *p* orbits surrounding 2α clusters (see Fig. 4). Itagaki *et al.* [11] have described the structures of ^{10}Be and ^{12}Be with an extended cluster model by assuming α cores and molecular orbits. In the study of Be isotopes with AMD methods [8,9,22], the structures with two α's and valence neutrons in neutron-rich Be isotopes have been microscopically confirmed without assuming the existence of any clusters or molecular orbits.

The single-particle wave functions and energies of an AMD intrinsic state are obtained by the definition described in Refs. [8,10]. By analyzing the ratio of the positive- and negative-parity components in each single-particle wave function, it is found that all of the neutron orbits are approximately parity eigenstates, which roughly correspond to the $1s$, $1p$, and $2s1d$ orbits. The lowest normal-parity $1/2^{-}$ state comes from a $0\hbar\omega$ configuration, because two neutrons occupy *s*-like orbits and the other five neutrons are in *p*-like orbits. On the other hand, in the ground $1/2^{+}$ state with the abnormal parity, the last neutron occupies a sd-like orbit, which means that the $1/2^{+}$ state is dominated by a $1\hbar\omega$ configuration. An interesting feature is found in the highest neutron wave function, which well corresponds to the sd-like orbit. The density distribution of neutrons is presented in Fig. 5(a). It has nodes along the longitudinal direction of 2α clusters and contains nearly 90% of a positive-parity eigenstate. It well corresponds to the so-called molecular σ orbit explained in the schematic of Fig. 4(a). On the other hand, the features of two neutron orbits energetically below the σ orbit are shown in Fig. 4(b). The dominating negative-parity component of these orbits indicates that the orbits correspond to *p*-like orbits. As shown in Fig. 5(b), the orbits seem to be similar to the molecular π orbits.

One of the reasons for parity inversion of ^{11}Be is considered to be because of the molecular σ orbit, which originates from sd orbits [6,30]. Since Be isotopes prefer to prolate deformations because of 2α clusters, the σ orbit can easily gain its kinetic energy in the clustering developed system. In other words, the 2α-cluster structure is one of advantages of the σ orbit in Be isotopes. The behavior of the single-particle wave functions of valence neutrons in the present results is almost consistent with the previous AMD studies [8,29].

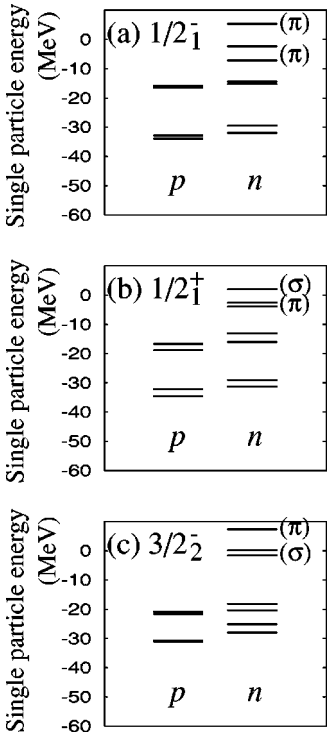

FIG. 6. Single-particle energies in the intrinsic system of (a) $1/2_1^-$, (b) $1/2_1^+$, and (c) $3/2_2^-$ with the case (1) interaction. The energies for protons (neutrons) are presented left (right) in each figure.

One of the new discoveries in the present work is that the possible negative-parity band $K^\pi = 3/2^-$ has a largely deformed shape with a remarkable cluster structure. With the same analysis of the single-particle wave functions as mentioned above, we find that two neutrons in the $3/2_2^-$ state occupy so-called σ orbits. In other words, the well-developed clustering is caused by these two neutrons in the σ orbits so as to gain their kinetic energies. It is surprising that such a $2\hbar\omega$ state appears in the low-energy region. The cluster structure in the $K^\pi = 3/2^-$ band is the very molecular structure which has been predicted by von Oertzen [6]. This is the first microscopic calculation which shows that such an exotic structure should exist in the low-energy region.

Figures 6(a), 6(b), and 6(c) show the single-particle energies in the intrinsic states of $1/2_1^-$, $1/2_1^+$, and $3/2_2^-$ with the case (1) interaction, respectively. The highest orbit in Fig. 6(b) corresponds to the σ orbit in the $1/2_1^+$ state. The energy of the intruder σ orbit is lower than the highest π orbit in the $1/2_1^-$. In all of the states ($1/2_1^-$, $1/2_1^+$, and $3/2_2^-$), the 2α cores consist of four neutrons and four protons in the $1s$-like orbits and the lower p-like orbits shown in Fig. 6. The small level spacing between the lower $1s$ orbits and the lower $1p$ orbits indicates the development of 2α clusters in the $1/2^+$ and $3/2_2^-$ states.

In the single-particle energies shown in Fig. 6(c), we find another interesting thing concerning the inversion between the σ orbits and an odd-neutron π orbit in the $3/2_2^-$ state. One of reasons for the higher energy of the odd-neutron π orbit than the σ orbits is a lack of pairing interaction because of the absence of another neutron in the π orbit. Another reason is degeneration between the σ orbits and the π orbits at a large intercluster distance. With the increase of the relative distance between 2α clusters, the σ orbits gain energy, while the π orbits lose potential energy. As the relative distance increases, the σ orbits cross the higher π orbits and come down near the lower π orbits. It is helpful to see the neutron level scheme of the two-center shell model [30] to understand the inversion of the π and the σ orbits with an increase of the intercluster distance.

TABLE III. Expectation values of the squared total intrinsic spin of protons S_p^2 in the excited states of ^{11}Be.

$J_n^\pm$ states	$0.5\times\langle S_p^2\rangle$ Case (1)	Case (2)
($K^\pi = 1/2^-$ band)		
$1/2_1^-$	0.07	0.04
$3/2_1^-$	0.1	0.04
$5/2_1^-$	0.2	0.04
($K^\pi = 3/2^-$ band)		
$3/2_2^-$	0.04	0.003
$5/2_2^-$	0.01	0.003
$7/2_2^-$	0.01	0.002
($K^\pi = 1/2^+$ band)		
$1/2_1^+$	0.03	0.01
$3/2_1^+$	0.02	0.01
$5/2_1^+$	0.03	0.01
$7/2_1^+$	0.02	0.01
$9/2_1^+$	0.02	0.004
$3/2_3^-$	0.7	1.0

As mentioned above, it is found that the origins of the drastic change between the rotational bands are the neutrons in the σ orbits and the π orbits surrounding the 2α cores. The intrinsic states are characterized by the number of valence neutrons in the σ orbit. That is to say, no neutron, one neutron, and two neutrons occupy the σ orbits in the $K^\pi = 1/2^-$, $1/2^+$, and $3/2^-$ bands, respectively. The deformation with the cluster structure is enhanced by the increase of the neutrons which occupy the σ orbits due to the energy gain of the σ orbits in the developed cluster structure.

C. Breaking of 2α cluster cores

Although the structures with 2α-cluster cores are seen in most of the states of ^{11}Be, the α clusters are not the ideal α clusters with simple $(0s)^4$ configurations. The α clusters are slightly broken because of the spin-orbit force. The components of cluster breaking allow β decays from ^{11}Li into ^{11}Be. This is a similar to that seen in the 3α-cluster structures of ^{12}C to which the Gamow-Teller transitions from ^{12}B and ^{12}N are not weak.

In the calculated results, we can know the degrees of breaking from the ideal 2α clusters by estimating the nonzero total intrinsic spin ($S_p \neq 0$) components for protons. If we neglect the $S_p \geqslant 2$ components and assume that only the $S_p = 0$ and $S_p = 1$ components are contained in a state, the

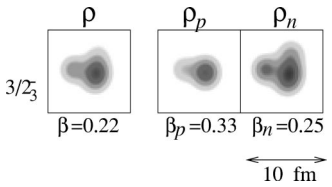

FIG. 7. Density distribution of the intrinsic wave function of $3/2_3^-$ calculated with the case (1) interaction.

value $0.5\times\langle S_p^2\rangle$ directly indicates the mixing ratio of the non-$(0s)^4$ configurations, which signifies the degree of cluster breaking in the state. In Table III, the expectation values of the squared total intrinsic spin of protons are listed. Generally speaking, the clustering breaking is larger in the results in case (1) than in case (2) because the stronger spin-orbit forces in case (1) give larger effects on the dissociation of 2α-cluster cores. The states $1/2_1^-$, $3/2_1^-$, and $5/2_1^-$ in $K^pi=1/2^-$ contain significant components of the cluster breaking in ratios of 7%, 10%, and 20%, respectively. The mixing of cluster breaking allows β decays into these states from ^{11}Li, which is consistent with experimental measurements (Table I). The smaller mixing in $1/2_1^-$ than in the other $3/2_1^-$, $5/2_1^-$ states is reflected by the relatively weak β decays to $1/2_1^-$, as mentioned in the previous section concerning the β-decay strength. On the other hand, the breaking of α clusters is very small in $K^pi=1/2^+$ and $K^\pi=3/2^-$, which have well-developed cluster structures. Therefore, the Gamow-Teller transitions to the excited states in the $K^\pi=3/2^-$ band from ^{11}Li are predicted to be weak, except for β decays to the $3/2_2^-$ state, because this state slightly contains cluster breaking due to state mixing with the lower $3/2_1^-$ state.

We discovered an excited $3/2_3^-$ state where the 2α-cluster structure is completely broken. In the density distribution of protons we cannot recognize the dumbbell shape in this state (see Fig. 7). As can be seen in Table III, the main component is the proton intrinsic spin $S_p=1$ state. As a result, the β-decay transitions from ^{11}Li to the $3/2_3^-$ state are strong compared with the β-decay strength to the other excited states of ^{11}Be. This is consistent with the strong β decays to the state at 8.04 MeV, which have recently been measured.

Although the 2α-core structures are dominant in most Be isotopes, it is interesting that the excited state with the complete breaking of one of the 2α's appears in neutron-rich Be. Even in the excited states with 2α cores, the components of the cluster breaking play an important role in the strength of β decays from ^{11}Li.

D. Parity inversion

We consider the details of parity inversion of the ground state in the case (1) calculations. Concerning the energy gain of the positive-parity $1/2^+$ state, the effects of the halo structure, the cluster structure with a prolate deformation, the three-body force, the angular momentum projection, and the pairing have been discussed in pioneering works [16].

In the present calculations the effects of the cluster structure were included as well as the pioneering AMD studies [16,22]. One of the reasons for parity inversion is the energy gain of the molecular σ orbit in the system with developed 2α clustering. The details of clustering and molecular orbits have already been mentioned above.

TABLE IV. Energies of the positive- and negative-parity states of ^{11}Be. The parity-projected AMD calculations with fixed intrinsic spins (a) before angular momentum projections, (b) after angular momentum projections of VBP within the perturbative treatment, and (c) results of the exact VAP calculations are listed. We also show (d) the present VAP calculations with variational intrinsic spins, but no diagonalization of the basis. The adopted interactions are the case (1) force. The energy difference δE between the positive- and negative-parity states is defined as $E_{1/2^+}-E_{1/2^-}$ for the calculations after angular momentum projections and $E(+)-E(-)$ before the projection.

Intrinsic spins	(a) Before projection Fixed	(b) VBP Fixed	(c) VAP Fixed	(d) VAP Variational parameters
^{11}Be(+)	−46.5	−53.1	−54.7	−57.1
^{11}Be(−)	−47.1	−52.0	−55.7	−57.0
δE	0.6	−1.1	1.0	−0.1

The three-body force was calculated approximately with a perturbative treatment in a pioneering study [16]. In the present work, the three-body force was treated exactly in the same way as the previous AMD study in Ref. [22].

In the previous AMD studies of ^{11}Be [16,22], the angular momentum projection was perturbatively treated. That is to say that the energy variation was performed after a parity projection, but before an angular momentum projection (VBP). Concerning the present results, we performed energy variation exactly for the spin-parity-projected wave functions (VAP). We then found that the effect of angular momentum projection on the parity inversion is quite different from the previous VBP results with perturbative treatments. In order to quantitatively discuss the effects, we estimate the energy difference between the $1/2^-$ and $1/2^+$ states: $\delta E\equiv E_{1/2^+}-E_{1/2^-}$. The parity inversion is described by a negative value of δE. The experimental value of δE has been known to be -0.32 MeV. For simplicity, we performed parity-projected AMD calculations with fixed intrinsic spins by using the case (1) interaction. In Table IV, the values of δE and energies (a) without angular momentum projections, (b) the angular momentum projections after variation within the perturbative treatments of VBP, and (c) results of the exact VAP calculations are listed. Before the angular momentum projections, δE is 0.6 MeV. After the projection within the perturbative treatments of VBP, δE becomes as small as -1.1 MeV. This is because the energy gain of the positive-parity state by the angular momentum projection is 1.7 MeV larger than the gain of the negative-parity state. The origin is the well-developed cluster structure in the former state compared with the latter state, because a deformed system generally gains much energy due to an angular momentum projection. The VBP results are consistent with those of previous AMD studies in Refs. [16,22]. However, when we exactly treated the angular momentum projection with VAP calculations we found a new aspect in the

effects on the energy gain. In the previous AMD studies, it was known that in many cases, the VAP results of low-lying states are not very much different from the VBP results. It is true in the $1/2^+$ state. However, this is not true in the $1/2^-$ state. In the VAP calculations, the negative-parity state gains as much energy as 8.6 MeV due to the angular momentum projection because the deformation of the $1/2^-$ state grows more in the VAP calculations than in the VBP calculations, so as to gain the energy of the angular-momentum-projected state. As a result, δE of (c) is 1.0 MeV, as much as the result before projections (a). In fact, the clustering of ^{11}Be($1/2_1^-$) is larger in the VAP results than expected in the VBP calculations. Therefore, the effect of the angular momentum projection is not positive for the parity inversion in ^{11}Be. This is one of new things in the present work which points to the conclusion that perturbative treatments of angular momentum projections do not always work well for precise descriptions.

Compared with the previous AMD studies of low-lying states of ^{11}Be [16,22], another improvement in the present framework is treating the intrinsic spin functions as variational parameters. In Table IV, the effect of flexible intrinsic spins is seen in the difference between (c) the VAP calculations with fixed intrinsic spins and (d) VAP calculations with the variational intrinsic spins. The treatment of flexible intrinsic spins has an important effect on the parity inversion of ^{11}Be. It reduces δE to a 1.1 MeV smaller value in (d) than that in the calculations (c). The importance of the flexible intrinsic spins in $p_{3/2}$ shell-closure states has already been argued in studies of ^{12}C [23] by one of the authors. In the case of ^{11}Be, it is natural to consider that the $p_{3/2}$ subshell effect is one of the reasons for the parity inversion, because the $p_{1/2}$ orbit should be raised relatively higher than the $2s_{1/2}$ orbits. Unfortunately, the simple AMD method with fixed intrinsic spins describes the subshell effects insufficiently. This is one of the advantages of the present framework, which can well describe both aspects of the clustering and shell effects.

Regarding the other reasons for parity inversion, Sagawa *et al.* [14] and Doté and Horiuchi [16] suggested the pairing effects in the neutron p shell. In the present framework, a part of the pairing effects in the p shell should be automatically included by spin-parity projections and superpositions.

As mentioned above, the clustering effects, the three-body forces, and the $p_{3/2}$ subshell effects are included in the present calculations. The pairing effects are expected to be partially contained. The other effect which should be important for parity inversion is the neutron-halo effect [13,16]. According to the study in Ref. [16], the effect due to the neutron-halo structure is estimated to be a 0.6 MeV reduction of δE. However, the halo effect was not taken into account in the present calculations. We think that this halo effect and the residual pairing effect are effectively contained in the strength parameter $u_{LS}=3700$ MeV of the spin-orbit force, which is slightly stronger that the parameter $u_{LS}=3000$ MeV adopted in Ref. [23]. The halo structures should be important only for the loosely bound states with low-spin orbits, such as s orbits and p orbits, at most. The present strong effective spin-orbit force in case (1) may artificially reduce too much the theoretical excitation energies of the other states in $K^\pi=1/2^+$ band, except for the $1/2^+$ state. Before concluding the relative position of the energies between the $K^\pi=1/2^-$ and $K^\pi=1/2+$ bands we should conduct more detailed research by taking the remaining effects, such as the halo structure, into consideration.

VI. SUMMARY

We studied the structures of the ground and excited states of ^{11}Be with VAP calculations within the framework of antisymmetrized molecular dynamics. Various kinds of excited states with cluster structures as well as noncluster structures were discovered in the theoretical results. We predicted many excited states. Most of the states belong to three rotational bands ($K^\pi=1/2^+$, $1/2^-$, and $3/2^-$), which are dominated by $1\hbar\omega$, $0\hbar\omega$, and $2\hbar\omega$ configurations, respectively. It should be pointed out that the formation of 2α-cluster cores is seen in many excited states of ^{11}Be in the the present results in spite of no assumption concerning the existence of clusters. The interesting point is that an eccentric rotational band $K^\pi=3/2^-$ with a mostly developed cluster structure starts from the $3/2_2^-$ state at about 4 MeV and reaches high-spin states.

The experimental data concerning the β^+-decay and β^--decay strength were reproduced well. We have also argued that cluster breaking plays an important role to allow β decays from ^{11}Li. The significant breaking of 2α cores in the states in the $K^\pi=1/2^-$ band has been seen while quantitatively estimating the breaking of clusters. We discovered a nonclustering state at about 10 MeV. One of the characteristics of this state is strong β decays from ^{11}Li, which well corresponds to the new excited states at 8.04 MeV found in the β^--decay measurements.

By analyzing the single-particle wave functions in the intrinsic states, it was found that the molecular σ orbits surrounding 2α cores play important roles in the cluster structures of ^{11}Be. In the ground band $K^\pi=1/2^+$, one neutron occupies the σ orbits. The newly predicted $K^\pi=3/2^-$ band is dominated by $2\hbar\omega$ configurations with two neutrons in the σ orbit. When the surrounding neutrons occupy the σ orbits, the clustering development is enhanced so as to gain kinetic energy. In other words, one of the reasons for the parity inversion and the low-lying $2\hbar\omega$ states is an energy gain of the σ orbits with the developed cluster structures.

Concerning the mechanism of parity inversion, we described the importance of molecular neutron orbits in the developed cluster structure and also mentioned the $p_{3/2}$ subshell effect. Although the spin parity of the ground state is described by a set of interaction parameters, case (1), we need more detailed research that takes the halo structures of the ground state into account.

ACKNOWLEDGMENTS

The authors would like to thank Dr. N. Itagaki and Dr. Doté for many discussions. They are also thankful to Professor W. von Oertzen for helpful discussions and comments. The computational calculations of this work are supported by the Supercomputer Project No. 58, No. 70 of High Energy Accelerator Research Organization (KEK), and Research Center for Nuclear Physics in Osaka University.

[1] A. A. Korsheninnikov *et al.*, Phys. Lett. B **343**, 53 (1995).
[2] N. Aoi *et al.*, Nucl. Phys. **A616**, 181c (1997).
[3] I. Daito *et al.*, Phys. Lett. B **418**, 27 (1998).
[4] M. Freer *et al.*, Phys. Rev. Lett. **82**, 1383 (1999); M. Freer *et al.*, Phys. Rev. C **63**, 034301 (2001).
[5] M. Milin *et al.*, Europhys. Lett. **48**, 616 (1999).
[6] W. von Oertzen, Z. Phys. A **354**, 37 (1996); **357**, 355 (1997).
[7] H. G. Bohlen, *et al.*, Nuovo Cimento A **111**, 841 (1998).
[8] A. Doté, H. Horiuchi, and Y. Kanada-En'yo, Phys. Rev. C **56**, 1844 (1997).
[9] Y. Kanada-En'yo, H. Horiuchi, and A. Doté, J. Phys. G **24**, 1499 (1998).
[10] Y. Kanada-En'yo, H. Horiuchi, and A. Doté, Phys. Rev. C **60**, 064304 (1999).
[11] N. Itagaki and S. Okabe, Phys. Rev. C **61**, 044306 (2000); N. Itagaki, S. Okabe, and K. Ikeda, *ibid.* **62**, 034301 (2000).
[12] Y. Ogawa, K. Arai, Y. Suzuki, and K. Varga, Nucl. Phys. **A673**, 122 (2000).
[13] H. Sagawa, Phys. Lett. B **286**, 7 (1992).
[14] H. Sagawa, B. A. Brown, and H. Esbensen, Phys. Lett. B **309**, 1 (1993).
[15] T. Otsuka, N. Fukunishi, and H. Sagawa, Phys. Rev. Lett. **70**, 1385 (1993).
[16] A. Doté and H. Horiuchi, Prog. Theor. Phys. **103**, 91 (2000).
[17] I. Ragnarsson, S. Aberg, H. B. Kansson, and R. K. Sheline, Nucl. Phys. **A361**, 1 (1981).
[18] M. Seya, M. Kohno, and S. Nagata, Prog. Theor. Phys. **65**, 204 (1981).
[19] S. Okabe, Y. Abe, and H. Tanaka, Prog. Theor. Phys. **57**, 866 (1977); S. Okabe and Y. Abe, *ibid.* **61**, 1049 (1979).
[20] K. Arai, Y. Ogawa, Y. Suzuki, and K. Varga, Phys. Rev. C **54**, 132 (1996).
[21] Y. Kanada-En'yo and H. Horiuchi, Prog. Theor. Phys. **93**, 115 (1995).
[22] Y. Kanada-En'yo, H. Horiuchi, and A. Ono, Phys. Rev. C **52**, 628 (1995); Y. Kanada-En'yo and H. Horiuchi, *ibid.* **52**, 647 (1995).
[23] Y. Kanada-En'yo, Phys. Rev. Lett. **81**, 5291 (1998).
[24] Y. Kanada-En'yo and H. Horiuchi, Prog. Theor. Phys. Suppl. **142**, 205 (2001).
[25] Y. Kanada-En'yo, in Proceedings of the Yukawa International Seminar 2001, Kyoto, 2001 [Prog. Theor. Phys. Suppl. (to be published)].
[26] T. Ando, K. Ikeda, and A. Tohsaki, Prog. Theor. Phys. **64**, 1608 (1980).
[27] N. Yamaguchi, T. Kasahara, S. Nagata, and Y. Akaishi, Prog. Theor. Phys. **62**, 1018 (1979); R. Tamagaki, *ibid.* **39**, 91 (1968).
[28] T. Suzuki and T. Otsuka, Phys. Rev. C **50**, R555 (1994).
[29] Y. Kanada-En'yo, Ph.D. thesis, Kyoto University, 1996.
[30] J. M. Eisenberg and W. Greiner, *Nuclear Theory I* (North-Holland, Amsterdam, 1975), p. 571.